Absorption Enhancement in "Giant" Core/Alloyed-Shell Quantum Dots for Luminescent Solar Concentrator

Haiguang Zhao, Daniele Benetti, Lei Jin, Yufeng Zhou, Federico Rosei,* and Alberto Vomiero**

***L**uminescent solar concentrators (LSCs) can potentially reduce the cost of solar cells by decreasing the photoactive area of the device and boosting the photoconversion efficiency (PCE). This study demonstrates the application of "giant" CdSe/$Cd_xPb_{1-x}S$ core/shell quantum dots (QDs) as light harvesters in high performance LSCs with over 1.15% PCE. Pb addition is critical to maximize PCE. First, this study synthesizes "giant" CdSe/$Cd_xPb_{1-x}S$ QDs with high quantum yield (40%), narrow size distribution (<10%), and stable photoluminescence in a wide temperature range (100–300 K). Subsequently these thick alloyed-shell QDs are embedded in a polymer matrix, resulting in a highly transparent composite with absorption spectrum covering the range 300–600 nm, and are applied as active material for prototype LSCs. The latter exhibits a 15% enhancement in efficiency with respect to 1% PCE of the pure-CdS-shelled QDs. This study attributes this increase to the contribution of Pb doping. The results demonstrate a straightforward approach to enhance light absorption in "giant" QDs by metal doping, indicating a promising route to broaden the absorption spectrum and increase the efficiency of LSCs.*

1. Introduction

The quest for high efficiency, low cost solar cells has prompted major research efforts, with the aim of identifying new materials with optimal spectral matching with solar radiation. In this context, colloidal quantum dots (QDs) have been recently explored for use in third generation excitonic solar cells, as well as other technologically relevant applications such as photodetectors, biosensors and light emitting devices.[1–6] In particular, QDs are being used to develop low cost solution processed solar cells, which could compete with current Silicon based technologies.[1,3] Near infrared (NIR) QDs are attractive materials for use in photovoltaics (PVs) applications due to their spectral tunability and the possibility of matching their absorption spectrum with sun light.[5] However, the PCE of QD-based cells is still quite low compared to that of commercial Silicon solar cells. In addition, the long-term stability is still a major challenge.[1]

A promising complementary approach to conventional PV systems is presented by luminescent solar concentrators (LSCs) that have been recently relaunched. Compared to traditional solar concentrators, LSCs can also be integrated in an urban environment thanks to their flexibility in terms of shape and color.[7] In LSCs, chromophores embedded in a planar waveguide (for instance a transparent polymer), absorb direct and diffused sunlight and re-emit concentrated light at a longer wavelength. The latter is collected in a PV cell placed at the edge of the waveguide, where it is

Dr. H. G. Zhao, D. Benetti, L. Jin, Y. Zhou, Prof. F. Rosei
Centre for Energy
Materials and Telecommunications
Institut National de la Recherche Scientifique
Université du Québec
1650 Boulevard Lionel-Boulet
Varennes, Québec J3X1S2, Canada
E-mail: haiguang.zhao@emt.inrs.ca; Federico.rosei@emt.inrs.ca
Prof. F. Rosei
Institute for Fundamental and Frontier Science
University of Electronic Science and Technology of China
Chengdu 610054, P. R. China
Prof. A. Vomiero
Department of Engineering Sciences and Mathematics
Luleå University of Technology
Luleå 971 98, Sweden
E-mail: alberto.vomiero@ltu.se

DOI: 10.1002/smll.201600945

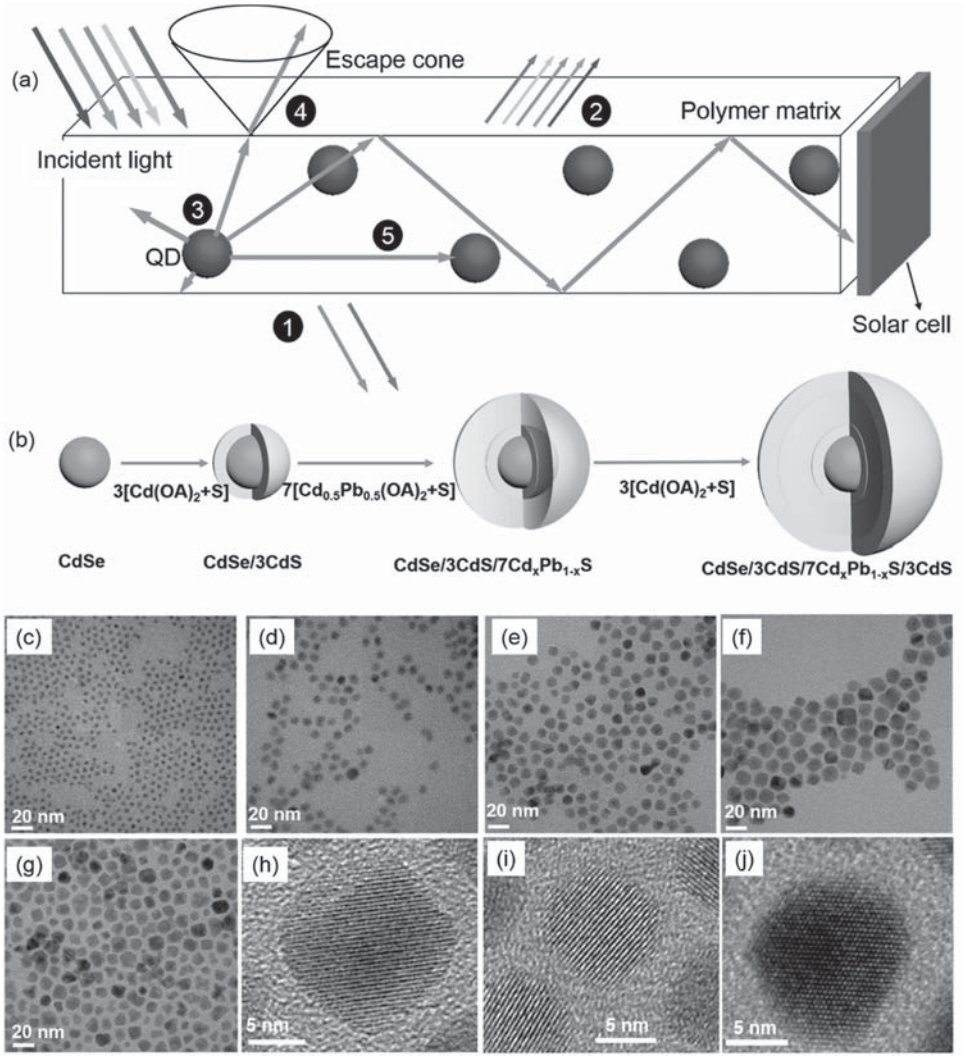

Figure 1. Schematic representation of a QD-based LSC and structure of QDs. a) LSC is obtained by embedding the QDs in a transparent polymer matrix. The numbers indicate the typical processes of energy loss in an LSC. 1) Unabsorbed light; 2) Light reflects from the top surface; 3) The light was absorbed by the QDs, but there is partial loss due to the non-unity of fluorescence QY; 4) Re-emitted incident light escapes from the surface due to the escape cone (the angle larger than the critical angle). 5) Light is reabsorbed by another QD. b) Scheme of the growth process for "giant" alloyed shell QDs. c) TEM.Representative TEM image of starting CdSe QDs before SILAR. d) CdSe QDs after coating with 3CdS/3Cd$_x$Pb$_{1-x}$S (3A), e) 3CdS/7Cd$_x$Pb$_{1-x}$S (7A), f) 3CdS/7Cd$_x$Pb$_{1-x}$S/3CdS (7A/3CdS), and g) 13CdS SILAR cycles. h) HR-TEM image of sample (g). i) HR-TEM image of sample (e). j) HR-TEM image of sample (f).

converted into electric power (**Figure 1**a).[8] One of the main limitations in LSCs is the reabsorption of the emitted light from the chromophores themselves, which impairs the final PCE of the device. QD-based LSCs are being studied as a new kind of LSC as they can significantly improve the overall PCE thanks to their high stokes shifts, which can significantly reduce light reabsorption. More importantly, they can significantly decrease the expensive PV module cost by exploiting their high quantum yield (QY), broad absorption spectrum, large absorption crosssections, size-tunable emission and enhanced chemical and photo stability with respect to most organic chromophores.[8–13]

In general, several factors can limit the PCE of LSCs. As shown in Figure 1a, light is lost in different ways (processes (1) to (5) in the scheme). (1) Only a fraction of incident light can be absorbed due to the limited overlap between the QD's absorption and solar spectra; (2) Part of the light is reflected at the front surface of the LSC; (3) Light is lost during re-emission, because the QY of the photoluminescence (PL) emission is below 100%; (4) The fraction of radiation which is re-emitted with an emission angle falling into the so-called escape cone cannot undergo total reflectance inside the waveguide and is lost[10]; (5) Part of the light is lost due to reabsorption (caused by the overlap between the absorption and emission spectra of the QDs).[8–10,13] Other minor light losses could be due to the absorption of emitted light by the polymer matrix. Among all the aforementioned processes of light loss, reabsorption from the QDs is one of the most critical issues in fabricating high efficiency large-scale LSCs.[9,10,13]

Several strategies have been proposed to eliminate self-absorption by increasing the Stokes-shift (the difference in wavelength between the positions of the band maxima of the absorption and emission spectra),[10] including the

use of heterostructured nanocrystals.[9,10,13] A successful approach involves the growth of doped semiconductor nanocrystals, which have demonstrated small LSC reabsorption losses,[13–15] for example, in Mn^{2+}-doped ZnSe QDs and Cu-doped CdSe QDs.[15] Unfortunately, this type of QD is affected by low QY (which limits photon emission) and critical long-term photo- and thermal-stability.[14,16]

Another approach is to coat the QDs with a wide bandgap semiconductor, which allows the formation of a quasi-type II bandgap alignment.[10] In this configuration, the electrons can typically leak into the shell region, while the holes are confined in the core of the structure, leading to spectral separation between emission and absorption.[9,10,17] In such heterostructured QDs, the shell/core volume ratio is very high and the shell material dominates the absorption properties. Red-shifted luminescence occurs either from the core or from the spatially indirect transitions across the heterointerface. The PCE of these heterostructured QD-based LSCs is still limited. For example, Meinardi et al. fabricated a large scale-LSC based on "giant" CdSe/CdS QDs embedded in poly(lauryl methacrylate-*co*-ethylene glycol dimethacrylate) (PMMA) polymer with PCE ≈1%.[10] One of the main limitations in the present "giant" QDs is the composition of the shell: to date, most giant QDs are coated with a thick CdS shell, for example, "giant" CdSe/CdS QDs, InP/CdS QDs, PbSe/CdSe/CdS QDs, Ge/CdS, etc.[10,18–21] As a consequence, the absorption spectrum is dominated by the shell, which strongly absorbs radiation below 500 nm (bandgap E_g of 2.49 eV) covering the UV and partially visible range, strongly limiting the application of LSCs in solar cells. It is very challenging to achieve high efficiency LSCs based on "giant" QDs with a thick CdS shell with absorption wavelengths above 500 nm, which calls for proper selection of shell materials and suitable coating techniques.

A promising solution might be to dope the CdS shell with a low bandgap semiconductor, to enhance the shell absorption and/or application of QDs, which are optically active in the NIR region.[4,14,16,22–25] The optical and electronic properties of QDs, such as absorption and PL can be controlled by tuning their composition and internal structure, without changing their overall size.[4,14,16,22–25] NIR emitting PbS QDs have been widely synthesized and their bandgap is as low as 0.41 eV (2.50 eV for CdS).[1,2,26] Importantly, the lattice mismatch between the CdS and rock salt PbS is very small, allowing the formation of a low defect alloyed $Cd_xPb_{1-x}S$ crystalline lattice.[2,26] For these reasons, both alloyed QDs and core/shell structures based on the combination of PbS and CdS are highly promising to obtain the desired optical properties in terms of absorption/emission in NIR, high spectral separation of absorption and emission and high QY. Obtaining composite QDs which absorb in the UV–vis–NIR spectral region and re-emitting in the NIR with large Stokes shift is still a challenge in the field, yet would represent a major advance. Taking into account that the incident photon to electron conversion efficiency (IPCE) of a standard Silicon solar cell is almost constant from 400 to 1000 nm, a QD-based LSC with a re-emission window in the NIR, at wavelengths below 1000 nm, would represent the perfect system to match the spectral features of a Silicon solar cell, integrated as a photon-to-electric power conversion device.

Here we demonstrate the application of "giant" CdSe/$Cd_xPb_{1-x}S$ core/shell QDs as active materials in high performance LSCs. First, we synthesized "giant" CdSe/$Cd_xPb_{1-x}S$ QDs via a successive ionic layer absorption and reaction (SILAR) approach, with high QY (40%), narrow size distribution (<10%) and wide-temperature PL stability (100–300 K). The presence of Pb in the CdS shell, in the form of rock salt PbS and $Cd_xPb_{1-x}S$ alloy with tunable concentration, was confirmed by both selected area electron diffraction (SAED) and X-ray photoelectron spectroscopy (XPS). These thick alloyed-shell QDs were embedded in a PMMA matrix, resulting in a highly transparent composite with low reabsorption losses, with the absorption spectrum ranging from 300 to 600 nm. The prototype LSC based on the alloyed shell exhibited a 15% enhancement in efficiency with respect to the pure CdS shell, up to 1.15% maximum efficiency thanks to the contribution of Pb dopants, higher than the highest efficiencies reported previously in Ref. [10]. These results indicate that Pb doping in CdSe/$Cd_xPb_{1-x}S$ core/shell QDs is a promising approach to fabricate high efficiency LSCs, with great potential for application in PV.

2. Results and Discussion

2.1. Synthesis and Structure of "Giant" Core/Shell QDs

CdSe QDs were synthesized according to procedures found in the literature.[27] A thick CdS shell was further grown by SILAR (see Section 4).[27] To enhance the absorption of QDs, we synthesized alloyed $Cd_xPb_{1-x}S$-shelled QDs with the same number of cycles as the CdSe/CdS QDs. Due to the lattice mismatch between the CdSe QDs (zinc-blend, ZB, 0.605 nm)[28] and PbS (rock salt, 0.593 nm) QDs,[26] which typically leads to the decrease of QY due to defects/traps, we first coated the CdSe core with three monolayers of CdS (CdSe/3CdS), then a mixture of Pb/Cd in a molar ratio of 1:1 was used to grow an alloyed $Cd_xPb_{1-x}S$ shell on the CdSe/3CdS QDs (Figure 1b), which can enhance the QY of the core from ≈8% to ≈80%. Finally, three additional monolayers of CdS were added on the alloyed shell to protect the QDs, aiming to improve the QY and chemical/photostability of QDs. The starting CdSe QDs have a core size of 3.27 nm in diameter with a uniform size distribution (standard deviation $\sigma < 10\%$) (Figure 1c and Figure 1 in the Supporting Information). A detailed analysis of QD core size and shell thickness is reported in **Table 1**. Increasing the number of SILAR cycles (transmission electron microscopy (TEM) analysis in Figure 1c–j) resulted in a quasi-linear increase of QD size (Table 1, Figures 1 and 2, Supporting Information). After the growth of 13 monolayers, the final diameter was 11.9 ± 0.8 nm for the CdSe/13CdS QDs (shell thickness ≈4.3 nm) and 12.6 ± 0.4 nm for the CdSe/3CdS/7$Cd_xPb_{1-x}S$/3CdS QDs (defined as CdSe/3CdS/7A/3CdS, shell thickness ≈4.7 nm) (Table 1). The crystal lattice is clearly visible by high resolution TEM imaging (Figure 1h–j).

Table 1. The overall size and shell thickness for investigated samples.

Sample	Structure	MLs	Overall size [nm]	Shell thickness [nm]
CdSe	CdSe	0	3.3 ± 0.2	0
CdSe/3A/3CdS	CdSe/3Cd$_x$Pb$_{1-x}$S/3CdS	3	7.7 ± 0.3	2.21
CdSe/3CdS/7A	CdSe/3CdS/7Cd$_x$Pb$_{1-x}$S	10	9.8 ± 0.4	3.29
CdSe/3CdS/7A/3CdS	CdSe/3CdS/7Cd$_x$Pb$_{1-x}$S/3CdS	13	12.6 ± 0.4	4.68
CdSe/13CdS	CdSe/13CdS	13	11.9 ± 0.7	4.29

Small-angle powder X-ray diffraction (XRD) was used to elucidate the various crystalline phases which are present in the QDs (**Figure 2**a). CdSe QDs exhibit a ZB structure, which is the typical crystalline phase of CdSe QDs grown at this temperature (300 °C).[17] The giant core/shell or core/alloyed shell nanocrystals after SILAR mainly exhibit the Wurtzite (WZ) structure, consistent with results obtained from SAED (Figure 3, Supporting Information).[17,27,29] There is no notable signal of ZB core in the XRD and SAED for 13-monolyer samples, due to the large volume percentage of CdS (>98%). Both energy-dispersive X-ray spectroscopy (EDS) in a single alloyed QD (CdSe/3CdS/7A) and XPS in alloyed QDs reveal the presence of elemental Pb, Cd, Se and S, indicating the successful inclusion of Pb in the CdS shell (Figure 2b, Figure 4, Supporting Information). For this sample, a cubic rock salt PbS phase is present in addition to the WZ CdS (Figure 5, Supporting Information). As we did not find any isolated PbS QDs during TEM analysis, this result further confirms the presence of a cubic rock salt PbS phase in the WZ CdS shell.

The Cd3d and Pb4f high resolution XPS spectra of the giant QDs are shown in Figure 2c,d and Figure 6 in the Supporting Information, confirming the presence of Cd and Pb in the alloyed-shell QDs. In particular, XPS allowed us to estimate the relative atomic ratio (R) of Cd/Pb (or doping concentration) of alloyed shell QDs. The ratio R is calculated by using CasaXPS software by comparing the ratio of the XPS peak area/relative sensitivity factor of the photoelectric peak. R is around 10 in the samples 3A and 7A and increases to 25 in sample 7A/3CdS (Figure 2e). As the XPS depth analysis

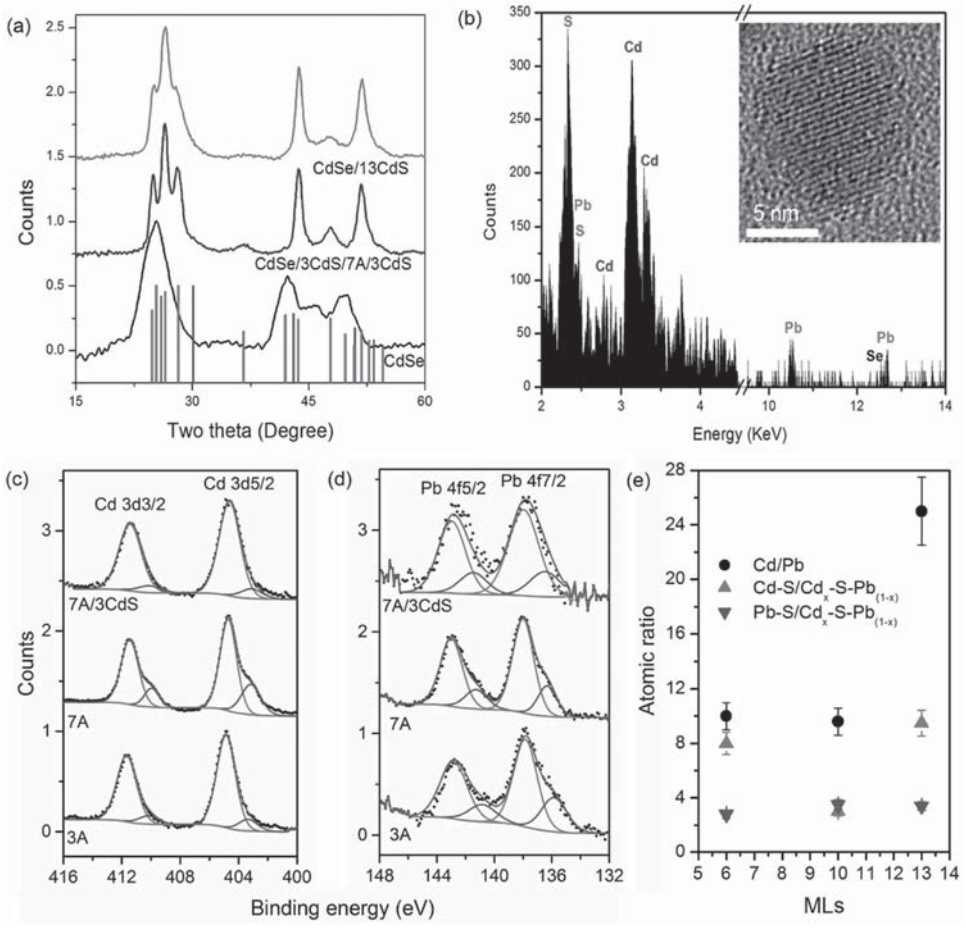

Figure 2. XRD patterns, EDX, and XPS spectra of QDs. a) XRD patterns of CdSe QDs before SILAR and after 13 cycle SILAR with CdS shell or alloyed shell. The JCPDS card files for PbS (001-0880, blue line) and CdS (01 080 0019, red for ZB and 01-077-2306, magenta for WZ) are shown for identification. b) EDX for a single CdSe/3CdS/7A QD. Inset of b) a single QD for EDX measurement. High resolution XPS spectra of c) Cd3d and d) Pb 4f in alloyed shell QDs. The dots represent the experimental data. The thick blue and red lines are the fitting components and the violet line is the overall fitting curve. The dark yellow line is a background curve. e) Atomic ratio of Cd/Pb, Cd—S/Cd$_x$—S—Pb$_{1-x}$ and Pb—S/Cd$_x$—S—Pb$_{1-x}$ as a function of the shell monolayers.

probes less than 3 nm, most of the signal originates from the surface of the QDs,[30] leading to a large increase of the Cd XPS signal in the 7A/3CdS sample. For samples 3A and 7A, instead, both Pb and Cd are present in the outer layer of the QDs, indicating that the Cd/Pb molar ratio (10:1) is reliable. The Cd3d 5/2 and Cd3d 3/2 spectra of CdSe QDs and CdSe/13CdS QDs exhibit two narrow peaks located at 404.8 and 411.3 eV, respectively, consistent with the binding energy of Cd−S and Cd−Se.[2] However, two additional components appear at 403.2 eV for Cd3d 5/2 and 409.9 eV for Cd3d 3/2 in the alloyed shell QDs (3A, 7A, and 7A/3CdS, respectively).

The main peaks located at 404.8 and 411.6 eV can be assigned to the chemical state of Cd−S, while the two additional peaks located at lower energy positions can be ascribed to a chemical state of Cd_x−S−Pb_{1-x} (Figure 2c), which leads to a decrease in binding energy.[30] The molar ratio Cd−S bond/Cd_x−S−Pb_{1-x} was estimated using the peak area ratio of Cd−S bond (red peak)/Cd_x−S−Pb_{1-x} bond (blue peak) (Figure 2e). With the increase of the alloyed monolayer from 3 (3A) to 7 (7A), the molar ratio decreases from 8 to 3 (Figure 2e), indicating an increase of alloyed (Cd_x−S−Pb_{1-x}) content as a function of alloyed monolayers, which confirms the presence of an alloyed structure in the "giant" QDs. Further coating of the 3-CdS layer (7A/3CdS) largely increases the molar ratio of Cd−S bond/Cd_x−S−Pb_{1-x} from 3 to 9.5 (Figure 2e) due to the addition of the Cd−S bond in the outer layer of CdS, which is the region which contributes the main XPS signal. For this sample, the signal does not originate only from the Cd 3d in the alloy, but mainly from the CdS out-layer (≈1 nm in thickness), leading to a decrease of Cd_x−S−Pb_{1-x} concentration. As Pb is only present in the alloyed shell, the Pb4f XPS signal will mainly originate from the Pb−S bond or Cd_x−S−Pb_{1-x} in the alloyed shell layer, while the Cd3d signal originates from both the out-CdS-layer and the alloyed layer. Consistent with the high resolution XPS spectra of Cd 3d, the high resolution XPS spectra of Pb 4f (Figure 2d) show the Pb 4f peaks from the Pb−S bond (137.9 and 142.9 eV), as well as Pb 4f peaks from Pb_{1-x}−S−Cd_x at 136.3 and 141.3 eV.[2] The relative atomic ratio of the two components (Pb−S/Pb_{1-x}−S−Cd_x) behaves similarly to that of Cd−S/Cd_x−S−Pb_{1-x} with ratio of ≈3–3.5:1, indicating that the alloyed shell is uniform in chemical composition. In addition, the present chemical state of Pb−S confirms the existing PbS cluster in the QDs, consistent with SAED results obtained from alloyed QDs (7A). The atomic concentration of the alloy (Pb_{1-x}−S−Cd_x) is quite close to (3:1) in both Cd3d and Pb4f high resolution spectra, due to the suitable detection depth (alloyed shell thickness of 3.3 nm) (Figure 2e). Based on the TEM, EDX, XRD and XPS results, we conclude that: i) the alloyed shell in the giant QDs is composed of a homogeneous alloyed $Cd_xPb_{1-x}S$ phase and pure PbS phase; ii) the relative molar ratio of Pb/Cd is 1:10, which is lower than the precursor feeding ratio of 1:1, indicating that the growth of the alloyed shell does not strictly follow a typical SILAR process. After feeding the mixture of $Pb(OA)_2$ and $Cd(OA)_2$ into the S-rich QDs, the reaction rate of Pb cations with S is faster than that of Cd cations, leading to the fast growth of the PbS phase, rather than the uniform alloyed structure ($Cd_{0.5}Pb_{0.5}S$). In addition, due to the different crystalline structure of PbS and CdS, they tend to segregate, rather than to form an alloyed structure during crystal growth. Such segregation mechanism is most probably responsible for the simultaneous presence of the PbS rock salt and the WZ CdS phases in the alloyed shell. However, the observation that the Pb/Cd ratio (1:10) in the sample is largely lower than the precursor ratio of Pb/Cd (1:1) is yet to be clarified. The difference in reaction rate of Pb and Cd, the different crystalline structure and the thermal stability might be the reasons. In fact, during the SILAR process, we found some precipitation on the wall of the reaction flask,[27] resulting in a final yield of QDs as only half of the pure CdS shell QDs with the same reaction cycles. Further detailed investigations are needed to improve the reaction yield by refining the reaction parameters.

2.2. Optical Properties of Giant QDs

The optical properties of QDs during the growth of the CdS shell are shown in **Figure 3**a–e. CdSe QDs show the first excitonic peak at 550 nm and the emission peak at 560 nm and a QY ≈8%. Then, coating the CdSe QDs with three monolayers of CdS, to avoid the lattice mismatch between CdSe and PbS results in significantly enhanced QY, from ≈8% to ≈80%, due to the improved surface passivation (Figure 3e).[27] Further growth of the alloyed shell via SILAR results in a variation in the PL FWHM and QY with respect to the pure shell QDs (see Figure 3d,e). The PL peak shows a typical red shift with respect to the original CdSe core due to the leakage of electrons from the core to the shell.[17,27] After a 13 cycle growth of the CdS shell via SILAR, the PL peak shows a 70 nm redshift (Figure 3a). The trends in the PL features of the Pb-doped shell (peak position and FWHM) are similar to the one of the pure CdS shell (Figure 3c,d). The QY of QDs after 7-cycle alloyed shell growth, instead, decreases to 17%, which is quite low compared with CdSe/CdS QDs with similar shell thickness (40%). The absorption spectrum of CdSe/13CdS QDs is dominated by the optical features of the shell, due to the larger shell volume compared to the core, even if the CdSe core absorption is still present (Figure 3a,b).

The absorption spectrum of the QDs presents an onset below 500 nm, corresponding to the CdS bulk bandgap (E = 2.50 eV).[28] Pb doping in the shell enhances shell absorption. The alloyed QDs still exhibits a first-excitonic absorption peak in the wavelength range 600–620 nm also in the giant QDs, with a pronounced absorption shoulder in the wavelength range 500–600 nm, which is not present in the CdSe/13CdS QDs. The bandgap energy for the alloyed shell ($Cd_xPb_{1-x}S$) was estimated by using the following equation, according to Vegard's Law[22,31]

$$E_g = E_{g(PbS)} \times (1-x) + E_{g(CdS)} \times x - b \times (1-x)$$

where E_g is the bandgap energy of the alloyed QD shell, $(1-x)$ and x are the percentage of PbS and CdS in the alloy, respectively, based on XPS measurements. $E_{g(CdS)}$ (2.50 eV) and $E_{g(PbS)}$ (0.41 eV) are the bulk bandgap energy of CdS

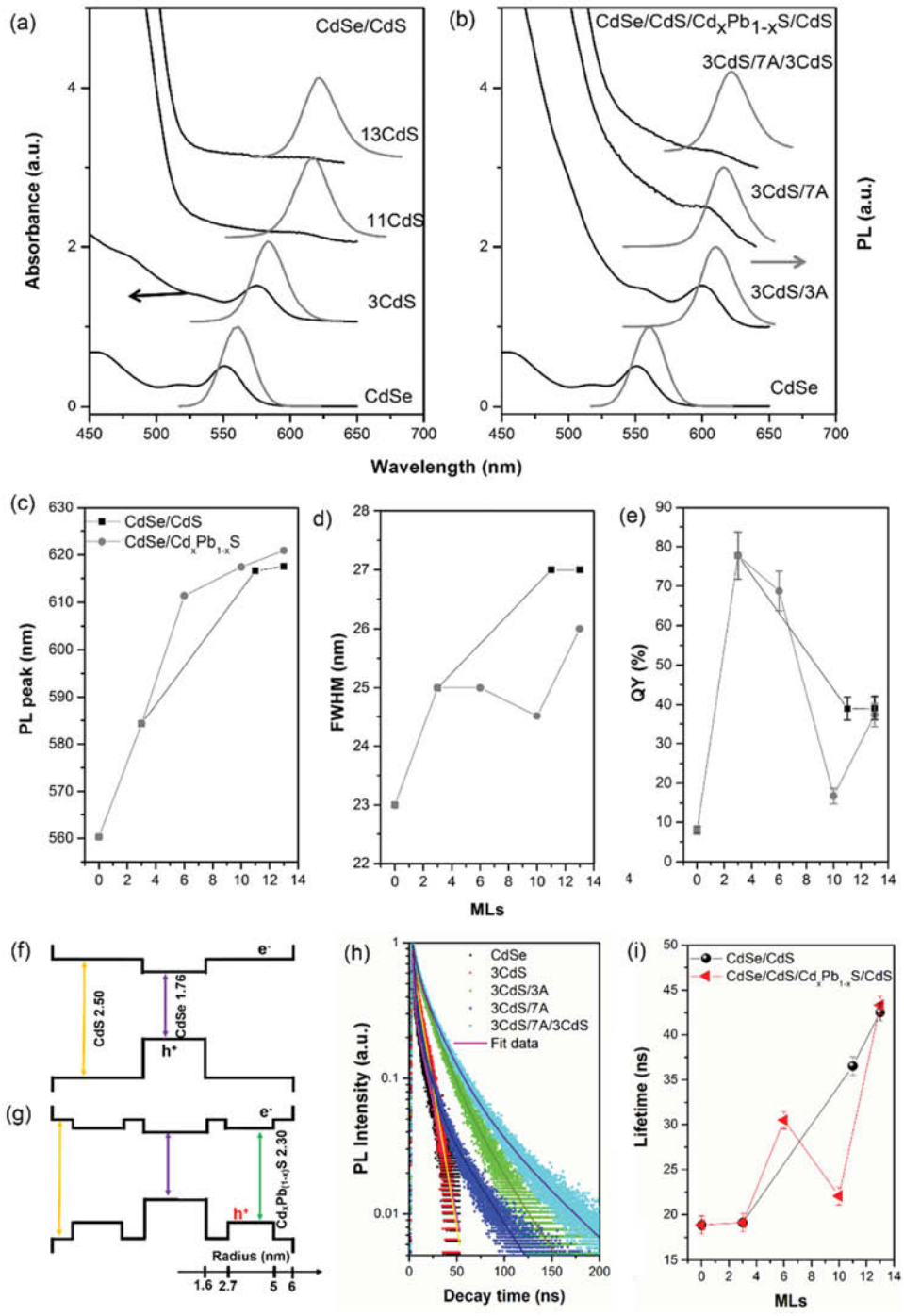

Figure 3. Optical properties of giant QDs. Absorption and PL spectra of CdSe QDs after coating with a) CdS shell or b) alloyed shell. c) PL peak position, d) FWHM, e) QY changes during the growth of QDs. Approximate relative energy band diagram of f) CdSe/13CdS QDs and g) CdSe/3CdS/7$Cd_xPb_{1-x}S$/3CdS QDs. A band alignment diagram of bulk CdSe (1.76 eV), CdS (2.50 eV),[28] and $Cd_xPb_{1-x}S$ (2.30 eV) indicated by the arrows in (h) and (i). h) Fluorescence decays and i) lifetimes of QDs in toluene for CdSe QDs for different shell coating. The excitation wavelength is $\lambda_{ex} = 444$ nm.

and PbS, respectively. The corresponding literature values for the parameter b were reported to be very small for Pb chalcogenide alloys (0.03–0.09)[22] and ≈0.45 for $CdSe_xS_{(1-x)}$ alloys.[32] The calculated band gap energy as a function of Cd concentration in the shell is reported in Figure 7 in the Supporting Information for values of b in the range 0–0.5. Due to the large concentration of Cd (90%), the calculated E_g is around 2.26–2.3 eV, with a very small contribution from b to the band energy for $Cd_xPb_{1-x}S$. Finally, the relative bandgap energy levels of the two different types of QDs are shown in Figure 3f,g. In principle, one can tune the bandgap of the alloyed shell by controlling the degree of doping (Figure 7, Supporting Information).[14,33] For example, the shell can absorb up to 850 nm wavelength, when $x = 0.5$ ($b = 0$).

However, the high concentration of Pb doping will lead to a large decrease in QY, due to the interactions between the localized electrons and holes, as suggested by Klimov and co-workers.[34] The QY of alloyed QDs can be enhanced by further coating the QD with three additional monolayers of CdS. The final QY in the alloyed giant QDs is comparable with that of the giant CdSe/CdS QDs, as high as 40% (Figure 3e). Considering the narrow FHWM (≈26 nm) and the high QY, the optical properties of our alloyed-shell QDs are comparable with the best values reported in the literature.[17,27] The increase of QY in the alloyed QDs can be explained by considering the role of the additional CdS shell in shaping their band structure. According to Figure 3f,g, in the alloyed QD with further CdS coating there might be a decreased hole leakage from the core to the external shell, compared with the alloyed QD before the external CdS shell, resulting in an increased QY.[34]

The PL lifetime of QDs of different shell structures was investigated through transient PL spectrometry under excitation at λ_{ex} = 444 nm, by focusing on the emission peak (Figure 3h,i). For all the samples, the decay curves can be fitted with a double exponential. The growth of thicker CdS shells results in an increase of lifetime from ≈18 ns (CdSe core) to ≈42 ns (13CdS). Since electrons in the CdSe core region can largely leak into the shell (Figure 3f,g), while the holes are still mostly confined in the core region, the decrease in electron–hole overlap can lead to a long recombination time between the electron and hole, resulting in the longer lifetime of the core/shell with respect to the original QDs, before shell growth.[10,17,29] However, the lifetime of seven monolayer alloyed shell QDs (3CdS/7A) behaves very differently from the pure CdS shell or other alloyed shell QDs. The lifetime in question is quite short (≈22 ns), which is consistent with the reduction in QY for this sample. The final lifetime of giant alloyed shell QDs with three layers of CdS is quite similar to the one of pure shell QDs due to the decrease in overlap between the electron and hole. In the giant core/shell QDs (CdSe core and CdS shell), the electron wave function exhibits an increasing leakage from the core to the shell region with increasing shell thickness, due to the relative energy alignment in the CdSe and CdS (Figure 3f) and the fact that the holes are still confined in the core region, which explains the shell-thickness dependent optical properties.[10,17,29] In the alloyed shell QDs, the shell layer has a bandgap energy of 2.3 eV, as shown in Figure 3g. The electron wave-function still leaks into the whole region of the shell due to the small difference in energy levels of either the pure CdS shell or the alloyed shell. However, benefiting from the favorable electronic band alignment, the hole can leak into the shell region (Figure 3g), similar to the possible hole leakage in giant CdSe/CdS QDs with an alloyed intermediate $CdS_xSe_{(1-x)}$ shell.[34] These phenomena result in a progressive increase of the electron–hole spatial overlap in the alloyed shelled QDs. As suggested by Brovelli et al., the increase of the electron–hole spatial overlap leads to a largely decreased QY and lifetime, which explains the optical behavior of the CdSe/3CdS/7A sample.[35] Further coating the CdS shell might modify the band alignment in alloyed shell QDs, and confine the hole in the core and alloyed shell regions, decreasing the electron–hole spatial overlap. Therefore, by engineering the structure and components of the shell, we can efficiently modify the optical properties of the alloyed shell QDs.

Figures 8 and 9 and Table 1 in the Supporting Information show the comparable PL enhancement factor, the temperature coefficients dE/dT and thermal activation energy, E_a in giant alloyed shell QDs[36–39] with respect to giant core/shell QDs suggests that the out-layer CdS shell coating on the alloyed shell QDs can significantly improve the thermal PL stability of alloyed shell QDs, making it suitable for further applications in solar energy conversion, such as solar cells and LSCs (a more detailed discussion for the thermal optical properties of QDs is illustrated in the Supporting Information).

2.3. "Giant" QD Based LSCs

To experimentally compare the efficiency, we fabricated large-area LSCs (7 cm × 1.5 cm × 0.3 cm) by embedding the "giant" QDs in a polymer matrix following a previously reported procedure (details shown in Section 4).[9,10] The geometric gain (the ratio of the surface areas of the top face and the edges, respectively) is ≈23, indicating a high optical concentration at the edge of the LSC. With respect to the pure CdS shell QDs, the alloyed shell QDs exhibit an enhanced absorption in the wavelength range 500–600 nm, especially for the QDs/polymer sample (**Figure 4**a), due to the Pb dopant in the shell. No significant changes in the PL peak position or PL FWHM were found for the investigated samples before (in solution) and after embedding the QDs into the polymer matrix. The comparison of QYs in solution and solid samples was obtained according to the consolidated methodology proposed by Klimov and co-workers[10] that estimates the relative QYs of QDs in solution and in film by considering the variations in lifetime measured by time-resolved PL spectroscopy.[10]

The QY can be expressed as

$$\mathrm{QY} = \frac{k_{et}}{k_{et} + k_{net}}$$

where k_{et} and k_{net} are the radiative and the non-radiative decay rate, respectively.

The measured lifetime is equal to

$$\tau = \frac{1}{k_{et} + k_{net}}$$

The PL dynamics of CdSe/13CdS or CdSe/3CdS/7A/3CdS QDs before (in solution) and after embedding into the polymer exhibit almost no variation in lifetimes (Figure 4c,d), indicating that the preparation process does not lead to the formation of a significant density of surface-defects/traps, which can highly affect the non-radiative decay rate, k_{net}.[9] Based on Klimov's assumption,[10] the polymerization process only affects k_{net} of QDs. Since the measured lifetime (τ) of the investigated "giant" QDs does not change after

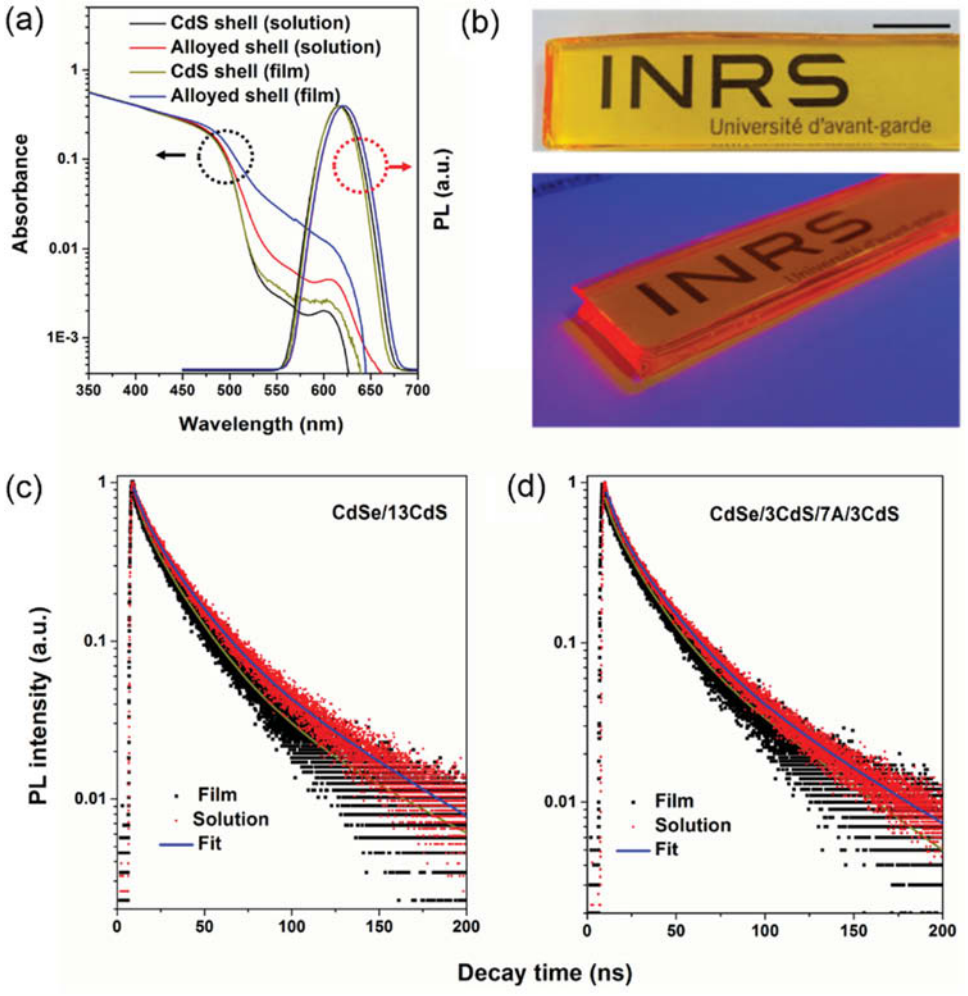

Figure 4. Optical properties in LSC. a) Absorption and normalized PL spectra of the QD in toluene solution and in polymer. PL spectra (excitation at 400 nm) were collected at the edge of the LSC when the excitation spot is located at 5 cm from the edge. b) Camera pictures of a QD–polymer-based LSC (dimensions: 7 cm × 1.5 cm × 0.3 cm) comprising CdSe/3CdS/7A/3CdS QDs illuminated under ambient illumination (top) and by an ultraviolet lamp emitting at 365 nm (bottom). Scale bar is 1 cm. Fluorescence decays of QDs in toluene or in the polymer for c) CdSe/13CdS QDs and d) CdSe/3CdS/7A/3CdS QDs. The excitation wavelength is $\lambda_{ex} = 444$ nm.

embedding them in the polymer, we can deduce that the factor $(k_{et} + k_{net})$ does not change either.

This is a clear indication that the "giant" QDs embedded in the polymer keep almost the same QY as in solution, highlighting the important role of a thick CdS or alloyed shell. Figure 4b presents camera pictures of one of the devices under ambient (top) and ultraviolet (bottom) illumination above the LSC. The LSC exhibits a good transparency and a high intensity red light on the edge.

Standardization of efficiency measurements in LSCs are still an open issue. For this reason, to allow a fair comparison of our results with previous achievements in the literature, in this study we applied the setup as described in Refs. [10,41,42]. The LSC was illuminated perpendicular to its surface by a 1.5 AM global solar simulator (100 mW cm^{-2}). We applied two different configurations for measuring the intensity output in the LSCs (**Figure 5**a,b). In the first scheme (Figure 5a), a standard Silicon solar cell was coupled with one of the edges of the LSC. In the second setup (Figure 5b), the output luminescent light on the edge of the LSC was collected by an optical fiber coupled with a standard power meter. Mirrors were added on the lateral sides and on the bottom of the LSC to limit photon losses.[7,40]

The theoretical optical efficiency of an LSC is defined as the number of photons emitted from the LSC edge over the total number of photons impinging on the LSC through the top surface. It can be calculated as

$$\eta_{opt} = (1-R)\,P_{TIR} \cdot \eta_{abs} \cdot \eta_{PLQY} \cdot \eta_{Stokes} \cdot \eta_{host} \cdot \eta_{self}$$

where R is the reflection of solar light from the waveguide surface, P_{TIR} is the total internal reflection efficiency, η_{abs} is the fraction of solar light that is absorbed by the dye, η_{PLQY} is the PL QY of QDs, η_{Stokes} is the energy lost due to heat generation during the absorption and emission event, η_{host} is the transport efficiency of the wave-guided photons through the waveguide, η_{TIR} is the reflection efficiency of the waveguide, and η_{self} is related to reabsorption of the emitted photons by another luminophore in the waveguide.

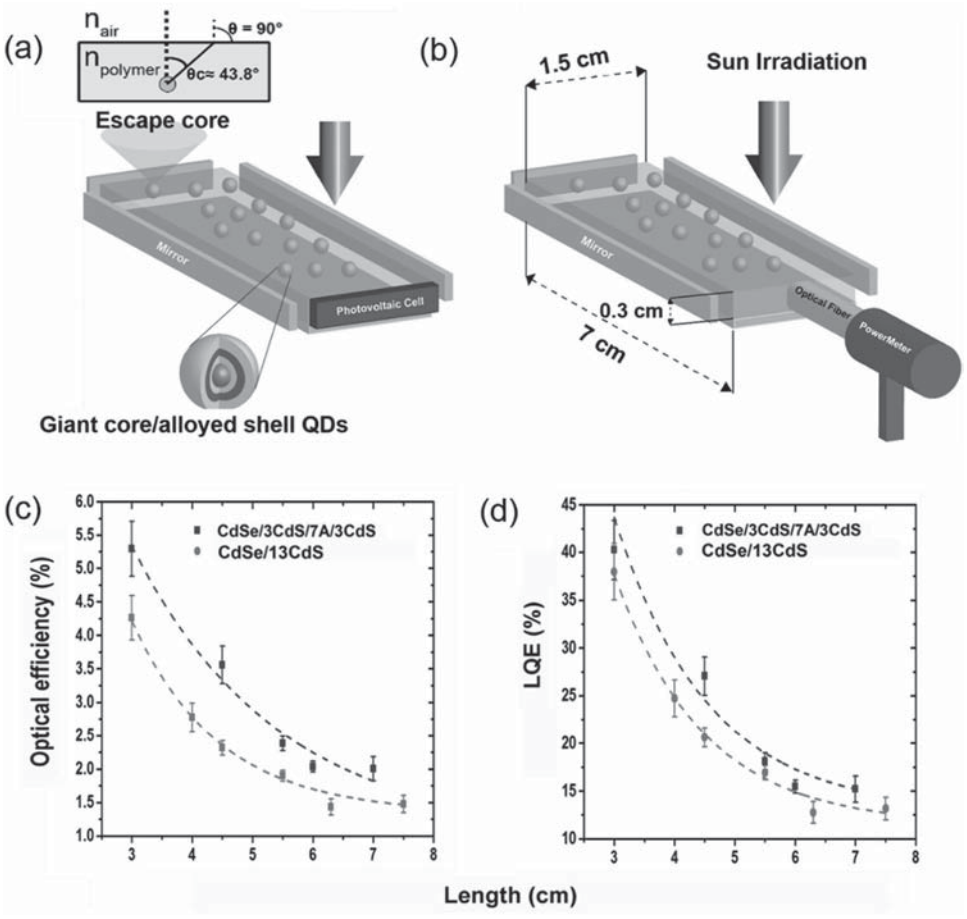

Figure 5. Optical efficiency in LSC. Scheme of the two different configurations used for characterizing the efficiency of the LSC. a) A Silicon cell (1.5×0.3 cm^2) is coupled with one edge of the LSC. b) An optical fiber collects the light from one edge of the LSC and its intensity is measured by a power meter. Dependence of c) the optical efficiency and d) LQE from the length. At $L = 3$ cm ($G = 10$) the maximum optical efficiency reached is 5.3% (for the alloyed QDs based LSC) and 4.3% for the CdSe/13CdS structure.

Considering the normal incidence of the simulated sunlight, we can estimate the fraction of the incident light reflected by the collecting surface as[41–43]

$$R = \frac{\left(n_{\text{polymer}} - n_{\text{air}}\right)^2}{\left(n_{\text{polymer}} + n_{\text{air}}\right)^2}$$

where n_{polymer} and n_{air} are the refractive index of polymer and air, respectively.

Thus, the fraction of incident light collected by the LSC is

$$1 - R = \frac{4n_{\text{polymer}}}{\left(n_{\text{polymer}} + n_{\text{air}}\right)^2}$$

In our case $n_{\text{polymer}} \cong 1.445$ giving a ≈97% of light collected.

It is also possible to estimate the total internal reflection efficiency P_{TIR}. The refractive index of the polymer (n_{polymer}) determines a critical angle θ_{C} above which total internal reflection occurs. Its value is

$$\theta_{\text{C}} = \sin^{-1}\left(\frac{n_{\text{air}}}{n_{\text{polymer}}}\right) \rightarrow \theta_{\text{c}} = 43.8\ ^\circ$$

Assuming an isotropic emission, P_{TIR} is defined by the solid angle (the so-called escape cone in Figure 4e) identified by the critical angle θ_{C}[41–43]

$$P_{\text{TIR}} = \sqrt{1 - \left(\frac{n_{\text{air}}}{n_{\text{polymer}}}\right)^2} \rightarrow P_{\text{TIR}} \cong 72.2\%$$

By applying the aforementioned scheme (Section 4), we focus on the calculation of the final optical efficiency, defined as the number of emitted photons at the output of the LSC divided by the number of incident photons impinging the top surface of the LSC.

A common method to estimate η_{opt} is to couple a calibrated PV cell at the end of the LSC.[7,44–48] In this case, η_{opt} can be calculated as

$$\eta_{\text{opt}} = \frac{I_{\text{LSC}} \cdot A_{\text{PV}}}{I_{\text{SC}} \cdot A_{\text{LSC}}} = \frac{I_{\text{LSC}}}{I_{\text{SC}} \cdot \text{G}}$$

where I_{LSC} is the short circuit current generated by the cell coupled to the LSC, I_{SC} is the short circuit current of the same PV cell under direct illumination, A_{PV} is the area of the edge of the LSC (or the active area on the PV cell, if the area

is smaller) and A_{LSC} is the area of the top of the LSC. The ratio A_{LSC}/A_{PV} is defined as the geometrical gain factor, G.

We calculated the luminescence quantum efficiency (LQE) based on η_{opt}. The LQE represents the number of photons emitted by the edge of the LSC over the number of photons absorbed by the LSC. We also measured directly the efficiency as the ratio P_{out}/P_{in}, where P_{out} is the light power at the edge of the LSC, and P_{in} is the light power impinging normal to the LSC's top surface.

Figure 5c reports the optical efficiency, calculated with the first method, for LSCs with different lengths. In general, LSCs realized with alloyed shell QDs have higher efficiencies compared to the CdSe/13CdS based LSC, with a maximum η_{opt} of 5.3% at L = 3 cm (G = 10) compared to 4.3% of the CdSe/13CdS structure, with an enhancement of ≈20%. As expected, increasing the geometrical factor reduces the efficiency for both devices, yet the LSC with alloyed shell QDs always maintains a higher efficiency due to the absorption enhancement.

The optical efficiency calculated using this methodology is based on the comparison of the J_{sc} generated by the reference solar cell coupled to the LSC, versus the J_{sc} generated by the reference cell under exposure to the full solar spectrum. A more significant comparison can be obtained by calculating the current generated by the Silicon cell under the same spectrum, in the absorption range similar to the spectrum emitted by the LSC.

The IPCE of the Silicon cell is almost constant in the range 300–1100 nm (Figure 10, Supporting Information). For this reason, it is possible to calculate the LQE of the LSC using the following formula

$$\eta_{LQE} = \frac{I_{LSC}}{I_{SC}^{Abs} \cdot G}$$

Where I_{SC}^{Abs} is the short circuit current of the PV cell calculated as

$$I_{SC}^{Abs} = I_{SC} \cdot \frac{\int P_\lambda A_\lambda \lambda \, d\lambda}{\int P_\lambda \lambda \, d\lambda}$$

where I_{SC} is the short circuit current of the PV cell under direct illumination, P_λ is the solar irradiance, and A_λ is the absorption spectrum of the LSC.

In Figure 5d we report the LQE for the LSC with the alloyed shell QDs and for the CdSe/13CdS device. The maximum efficiency is 40% for the CdSe/7A/13CdS LSC for L = 3 cm (G = 10) and 15.2% for L = 7 cm (G = 23). Compared to the LSC without the alloyed shell, the enhancement is in the 7% to 32% range (at L = 4.5 cm/G = 15). The maximum efficiency (40%) is in good agreement with our measured QY of QDs in solution, indicating that the fabrication process does not affect the QY. These values are comparable with the highest values reported in the literature for a similar system with CdSe/CdS QDs.[9,10] The difference between our result and previous work is that in our case we use a modified shell, doped with Pb. Using this strategy, we obtained a maximum efficiency close to the QY, comparable to the best η_{opt} of 40% using QDs with a fluorescence QY double (around 80%) and a device almost three times smaller.[9] Compared to a large-area LSC with G = 40 with an optical efficiency of 10%,[10] our system can theoretically reach an efficiency of ≈8.5% at G = 40 (L = 12 cm) (based on the exponential fitting of our experimental results).

To exclude the dependence of the LSC performance from the Silicon solar cell, the efficiency was then calculated using the second method, obtaining the ratio P_{out}/P_{in}. The test was performed on LSCs with geometrical factor equal to 23 (7.0 cm × 1.5 cm × 0.3 cm). The efficiency (η) was calculated as the ratio P_{out}/P_{in}, where P_{out} is the power on the edge and P_{in} is the power coming into the LSC. Based on these measurements, we find η of 1.2% for CdSe/13CdS based LSC, which is comparable with the reported efficiency of similar type QDs–LSC.[10] In the LSC based on the alloyed shell QDs, η goes up to 1.4%, with over 15% enhancement, consistent with the increase in optical efficiency. This improvement in alloyed shell QDs measured by power meter is consistent with the results from the first method using a Silicon solar cell.

3. Conclusions and Perspectives

We synthesized "Giant" CdSe/$Cd_xPb_{1-x}S$ core/shell QDs with high QY (40%), narrow size distribution (<10%) and good thermal stability by controlling Pb doping via the SILAR approach. These thick alloyed-shell QDs were integrated into LSCs, which exhibit low reabsorption losses due to an increase in the Stokes shift. In addition, the alloyed shell QDs show an enhanced absorption spectrum in the 300–600 nm range compared to pure shell QDs. The prototype LSC based on the alloyed shell exhibited a ≈15% enhancement in efficiency with respect to the pure CdS shell, thanks to the contribution of the Pb dopant. The doping of the QDs enhances the LSC efficiency close to the QY, reaching values similar to the highest efficiencies reported for a low-reabsorption CdSe/CdS QDs system. The demonstrated metal doping approach can be applied to other "giant" colloidal QDs systems, such as InP/CdS or PbSe/CdSe/CdS QDs. In addition, the refined Pb doping concentration can tune the absorption spectra of QDs to better match the solar spectrum, and can represent a significant advance for the development of high-efficiency LSCs for cost-effective PV applications.

4. Experimental Section

Materials: Lead(II) acetate trihydrate, sulfur (100%), oleylamine (OLA) (technical grade, 70%), cadmium oxide (99%), oleic acid (OA), Rhodamine 6G and octadecene (ODE), selenium pellet (≥99.999%), trioctyl phosphine oxide (TOPO), trioctyl phosphine (TOP) (97%), lauryl methacrylate, ethylene glycol dimethacrylate, diphenyl(2,4,6-trimethylbenzoyl)phosphine oxide, hexane, toluene, and ethanol were obtained from Sigma-Aldrich Inc. All chemicals were used as purchased.

Synthesis of CdSe QDs and "Giant" Core/Shell QDs: CdSe QDs were synthesized by using the hot injection approach.[27] Deposition of CdS layers on CdSe QDs followed the procedure described

in Ghosh et al.[27] Typically, in a 100 mL round-bottom flask, OLA (5 mL), ODE (5 mL) and CdSe QDs (≈2×10^{-7} mol in hexane) were degassed at 110 °C for 30 min. The reaction flask was restored with N_2 and the temperature was further raised to 240 °C with stirring. The $Cd(OA)_2$ dispersed in ODE (0.25 mL, 0.2 M) was added dropwise and the mixture was allowed to react for 2.5 h, followed by dropwise addition of 0.2 M sulfur in ODE with same volume. The shell was further annealed for 10 min. All subsequent shells were annealed at 240 °C for ≈10 min following the injection of sulfur and ≈2.5 h following dropwise addition of the $Cd(OA)_2$ in ODE. Sulfur/$Cd(OA)_2$ addition volumes for shell addition cycles 1–13 were as follows: 0.25, 0.36, 0.49, 0.63, 0.8, 0.98, 1.18, 1.41, 1.66, 1.92, 2.2, 2.51, and 2.8 mL, respectively. For the growth of the alloyed shell QDs, the mixture of $Cd(OA)_2$/$Pb(OA)_2$ (molar ratio of 1:1 with total concentration of 0.2 M) was used for the further growth of the shell until seven layers were completed. After that, another three CdS layers were coated on the alloyed shell. The reaction was cooled to room temperature using ice water. Ethanol was added, and then the suspension was centrifuged and the supernatant was removed. The QDs were then dispersed in toluene for further characterization.

Fabrication of LSCs: The LSCs were fabricated by embedding the QDs in the polymer matrix.[9,10] Typically, "giant" QDs dispersed in toluene or hexane were added to the 50 mL flask. The solvents were pumped away by a vacuum pump, then nitrogen flux was reestablished into the flasks. The monomer precursors of lauryl methacrylate and ethylene glycol dimethacrylate were mixed at a mass loading of approximately 20%. Then the resulting solution was mixed with a UV initiator (diphenyl(2,4,6-trimethylbenzoyl)phosphine oxide) and sonicated until a clear solution was formed. The solution was then injected into the flask containing the dried QDs powder. The mixture was homogeneously dispersed by ultrasound treatment and then injected into a mold consisting of two glass slides separated by a rubber spacer. The mixture was then illuminated with a UV lamp for 2 h.

Characterization: TEM characterization of the QDs was carried out with a JEOL 2100F TEM equipped with EDS and SAED. The small angle powder XRD study was performed with a Philips X'pert diffractometer using a Cu Kα radiation source ($\lambda = 0.15418$ nm). XPS was performed in a VG Escalab 220i-XL equipped with an Al Kα source. Absorption spectra were acquired with a Cary 5000 UV–vis–NIR spectrophotometer (Varian) with a scan speed of 600 nm min^{-1}. Fluorescence spectra were taken with a Fluorolog-3 system (Horiba Jobin Yvon). The PL lifetime of the QDs was measured in the time-correlated single-photon counting mode with a 444 nm laser. QY measurements for QDs were measured by using Dye rhodamine 6G as a reference.

The temperature-dependent optical properties of QDs were measured in the polymer matrix in the temperature range 100–300 K using THMS 600 temperature controlled stages.

The efficiency of LSCs was measured by using an ABET2000 solar simulator at AM 1.5G (100 mW cm^{-2}) calibrated using a reference Silicon cell and mechanical filters. During the measurement, a fiber was used to collect the emission in the edge of LSC, then the light intensity was measured using a power meter. In the other setup, a Silicon solar cell (IXYS KXOB22) was positioned at the end of the LSC. The current–voltage (*I–V*) characteristics of the fabricated LSC was measured by a Keysight 2900A SourceMeter under simulated sunlight using an ABET2000 solar simulator at AM1.5G (100 mW cm^{-2}) calibrated using a reference Silicon cell and mechanical filters.

Supporting Information

Supporting Information is available from the Wiley Online Library or from the author.

Acknowledgements

F.R. acknowledges FQRNT for funding through team projects, NSERC for a Discovery Grant and funding from MDEIE for an international collaboration grant with the European Network WIROX. A.V. is thankful to the European Union for partial salary support under contract No. 299490, MCIOF and for partial funding under contract No. 295216, IRSES. F.R. is grateful to NSERC for funding and partial salary support through an EWR Steacie Memorial Fellowship and the Alexander von Humboldt Foundation for a FW Bessel Award and Elsevier for a grant from Applied Surface Science. A.V. is grateful to Kempe Foundation and to LTU Labbfond program for equipment funds.

[1] S. A. McDonald, G. Konstantatos, S. G. Zhang, P. W. Cyr, E. J. D. Klem, L. Levina, E. H. Sargent, *Nat. Mater.* **2005**, *4*, 138.
[2] H. G. Zhao, D. F. Wang, T. Zhang, M. Chaker, D. L. Ma, *Chem. Commun.* **2010**, *46*, 5301.
[3] M. R. Kim, D. L. Ma, *J. Phys. Chem. Lett.* **2015**, *6*, 85.
[4] J. Lim, B. G. Jeong, M. Park, J. K. Kim, J. M. Pietryga, Y. S. Park, V. I. Klimov, C. Lee, D. C. Lee, W. K. Bae, *Adv. Mater.* **2014**, *26*, 8034.
[5] C. H. M. Chuang, P. R. Brown, V. Bulovic, M. G. Bawendi, *Nat. Mater.* **2014**, *13*, 796.
[6] M. F. Frasco, N. Chaniotakis, *Sensors* **2009**, *9*, 7266.
[7] M. G. Debije, P. P. C. Verbunt, *Adv. En. Mater.* **2012**, *2*, 12.
[8] A. J. Chatten, K. W. J. Barnham, B. F. Buxton, N. J. Ekins-Daukes, M. A. Malik, *Semiconductors* **2004**, *38*, 909.
[9] I. Coropceanu, M. G. Bawendi, *Nano Lett.* **2014**, *14*, 4097.
[10] F. Meinardi, A. Colombo, K. A. Velizhanin, R. Simonutti, M. Lorenzon, L. Beverina, R. Viswanatha, V. I. Klimov, S. Brovelli, *Nat. Photonics* **2014**, *8*, 392.
[11] D. Chemisana, *Ren. Sust. En. Rev.* **2011**, *15*, 603.
[12] M. J. Currie, J. K. Mapel, T. D. Heidel, S. Goffri, M. A. Baldo, *Science* **2008**, *321*, 226.
[13] Z. Krumer, S. J. Pera, R. J. A. van Dijk-Moes, Y. Zhao, A. F. P. de Brouwer, E. Groeneveld, W. G. J. H. M. van Sark, R. E. I. Schropp, C. d. M. Donega, *Sol. Energy Mater. Sol. Cells* **2013**, *111*, 57.
[14] J. D. Bryan, D. R. Gamelin, in *Progress in Inorganic Chemistry*, Vol. *54* (Ed: K. D. Karlin), John Wiley & Sons, Inc., Hoboken, NJ, USA, **2005**, p. 47.
[15] C. S. Erickson, L. R. Bradshaw, S. McDowall, J. D. Gilbertson, D. R. Gamelin, D. L. Patrick, *ACS Nano* **2014**, *8*, 3461.
[16] M. D. Regulacio, M.-Y. Han, *Acc. Chem. Res.* **2010**, *43*, 621.
[17] Y. Chen, J. Vela, H. Htoon, J. L. Casson, D. J. Werder, D. A. Bussian, V. I. Klimov, J. A. Hollingsworth, *J. Am. Chem. Soc.* **2008**, *130*, 5026.
[18] A. M. Dennis, B. D. Mangum, A. Piryatinski, Y. S. Park, D. C. Hannah, J. L. Casson, D. J. Williams, R. D. Schaller, H. Htoon, J. A. Hollingsworth, *Nano Lett.* **2012**, *12*, 5545.

[19] D. C. Lee, I. Robel, J. M. Pietryga, V. I. Klimov, *J. Am. Chem. Soc.* **2010**, *132*, 9960.
[20] K. P. Acharya, H. M. Nguyen, M. Paulite, A. Piryatinski, J. Zhang, J. L. Casson, H. W. Xu, H. Htoon, J. A. Hollingsworth, *J. Am. Chem. Soc.* **2015**, *137*, 3755.
[21] Y. J. Guo, C. E. Rowland, R. D. Schaller, J. Vela, *ACS Nano* **2014**, *8*, 8334.
[22] D. K. Smith, J. M. Luther, O. E. Semonin, A. J. Nozik, M. C. Beard, *ACS Nano* **2011**, *5*, 183.
[23] L. A. Swafford, L. A. Weigand, M. J. Bowers, J. R. McBride, J. L. Rapaport, T. L. Watt, S. K. Dixit, L. C. Feldman, S. J. Rosenthal, *J. Am. Chem Soc.* **2006**, *128*, 12299.
[24] R. Wang, O. Calvignanello, C. I. Ratcliffe, X. Wu, D. M. Leek, M. B. Zaman, D. Kingston, J. A. Ripmeester, K. Yu, *J. Phys. Chem. C.* **2009**, *113*, 3402.
[25] A. C. A. Silva, S. W. da Silva, P. C. Morais, N. O. Dantas, *ACS Nano.* **2014**, *8*, 1913.
[26] H. G. Zhao, M. Chaker, N. Q. Wu, D. L. Ma, *J. Mater. Chem.* **2011**, *21*, 8898.
[27] Y. Ghosh, B. D. Mangum, J. L. Casson, D. J. Williams, H. Htoon, J. A. Hollingsworth, *J. Am. Chem. Soc.* **2012**, *134*, 9634.
[28] C. Y. Moon, S. H. Wei, Y. Z. Zhu, G. D. Chen, *Phys. Rev. B.* **2006**, *74*, 233202.
[29] M. Cirillo, T. Aubert, R. Gomes, R. Van Deun, P. Emplit, A. Biermann, H. Lange, C. Thomsen, E. Brainis, Z. Hens, *Chem. Mater.* **2014**, *26*, 1154.
[30] K. Huang, R. Demadrille, M. G. Silly, F. Sirotti, P. Reiss, O. Renault, *ACS Nano* **2010**, *4*, 4799.
[31] P. Reiss, M. Protiere, L. Li, *Small* **2009**, *5*, 154.
[32] P. P. Ingole, G. B. Markad, D. Saraf, L. Tatikondewar, O. Nene, A. Kshirsagar, S. K. Haram, *J. Phys. Chem. C* **2013**, *117*, 7376.
[33] D. Mourad, G. Czycholl, C. Kruse, S. Klembt, R. Retzlaff, D. Hommel, M. Gartner, M. Anastasescu, *Phys. Rev. B.* **2010**, *82*, 165204.
[34] W. K. Bae, L. A. Padilha, Y. S. Park, H. McDaniel, I. Robel, J. M. Pietryga, V. I. Klimov, *ACS Nano* **2013**, *7*, 3411.
[35] S. Brovelli, R. D. Schaller, S. A. Crooker, F. Garcia-Santamaria, Y. Chen, R. Viswanatha, J. A. Hollingsworth, H. Htoon, V. I. Klimov, *Nat. Commun.* **2011**, *2*, 280.
[36] P. T. Jing, J. J. Zheng, M. Ikezawa, X. Y. Liu, S. Z. Lv, X. G. Kong, J. L. Zhao, Y. Masumoto, *J. Phys. Chem. C.* **2009**, *113*, 13545.
[37] D. Valerini, A. Creti, M. Lomascolo, L. Manna, R. Cingolani, M. Anni, *Phys. Rev. B.* **2005**, *71*, 235409.
[38] K. A. Abel, H. J. Qiao, J. F. Young, F. van Veggel, *J. Phys. Chem. Lett.* **2010**, *1*, 2334.
[39] H. G. Zhao, H. Y. Liang, F. Vidal, F. Rosei, A. Vomiero, D. L. Ma, *J. Phys. Chem. C.* **2014**, *118*, 20585.
[40] M. G. Debije, J.-P. Teunissen, M. J. Kastelijn, P. P. C. Verbunt, C. W. M. Bastiaansen, *Sol. En. Mater. Sol. Cells.* **2009**, *93*, 1345.
[41] A. H. Z. J. S. Batchelder, T. Cole, *Appl. Opt.* **1979**, *18*, 3090.
[42] S. McDowall, T. Butler, E. Bain, K. Scharnhorst, D. Patrick, *Appl. Opt.* **2013**, *52*, 1230.
[43] J. Roncali, F. Garnier, *Appl. Opt.* **1984**, *23*, 2809.
[44] J. L. Banal, K. P. Ghiggino, W. W. H. Wong, *Phys. Chem. Chem. Phys.* **2014**, *16*, 25358.
[45] S. Flores Daorta, A. Proto, R. Fusco, L. Claudio Andreani, M. Liscidini, *Appl. Phys. Lett.* **2014**, *104*, 153901.
[46] J. Bomm, A. Büchtemann, A. J. Chatten, R. Bose, D. J. Farrell, N. L. A. Chan, Y. Xiao, L. H. Slooff, T. Meyer, A. Meyer, W. G. J. H. M. van Sark, R. Koole, *Sol. En. Mater. Sol. Cells* **2011**, *95*, 2087.
[47] H. Hernandez-Noyola, D. H. Potterveld, R. J. Holt, S. B. Darling, *Energy Environ. Sci.* **2012**, *5*, 5798.
[48] Y. Zhou, D. Benetti, Z. Fan, H. Zhao, D. Ma, A. O. Govorov, A. Vomiero, F. Rosei, *Adv. En. Mater.* **2016**, *6*, 1501913.

Received: March 18, 2016
Revised: June 20, 2016
Published online: August 12, 2016

